



Deposited via The University of Leeds.

White Rose Research Online URL for this paper:

<https://eprints.whiterose.ac.uk/id/eprint/190530/>

Version: Accepted Version

---

**Article:**

Wang, Q, Shen, J, Glover, PWJ et al. (2022) Improving the Prediction of Production Loss in Heterogeneous Tight Gas Reservoirs Using Dynamic Threshold Pressure. *Energy and Fuels*, 36 (19). pp. 11991-12003. ISSN: 0887-0624

<https://doi.org/10.1021/acs.energyfuels.2c02713>

---

This is an author produced version of an article published in *Energy and Fuels*. Uploaded in accordance with the publisher's self-archiving policy.

**Reuse**

Items deposited in White Rose Research Online are protected by copyright, with all rights reserved unless indicated otherwise. They may be downloaded and/or printed for private study, or other acts as permitted by national copyright laws. The publisher or other rights holders may allow further reproduction and re-use of the full text version. This is indicated by the licence information on the White Rose Research Online record for the item.

**Takedown**

If you consider content in White Rose Research Online to be in breach of UK law, please notify us by emailing [eprints@whiterose.ac.uk](mailto:eprints@whiterose.ac.uk) including the URL of the record and the reason for the withdrawal request.

# Improving prediction of production loss in heterogeneous tight gas reservoirs using dynamic threshold pressure

Qian Wang<sup>1\*</sup>, Jian Shen<sup>1</sup>, Paul W.J. Glover<sup>2</sup>, Piroska Lorinczi<sup>2</sup>, Ian Duncan<sup>3</sup>

<sup>1</sup> School of Resources and Geosciences, China University of Mining and Technology, Xuzhou, 221000, China

<sup>2</sup> School of Earth and Environment, University of Leeds, Leeds, LS2 9JT, UK

<sup>3</sup> Bureau of Economic Geology, The University of Texas at Austin, Austin, Texas 78713

\*Corresponding Author, Qian Wang, wqian6200@cumt.edu.cn

8  
9

**Abstract:** Tight gas reservoirs commonly exhibit complex pore-throat structures which lead to strong heterogeneity and anisotropy in their permeability tensors. Conventionally, a constant threshold pressure gradient (TPG) has been used to predict the production loss that arises from overcoming the rock's disinclination to flow water and gas through such complex pore-throat structures. The problem is that the TPG is not constant during the production lifetime of a reservoir. In this work we find that using a constant TPG results in large underestimations of gas production. This is because TPG varies significantly with both effective stress and water saturation; an effect which is greater for tight heterogeneous rocks. The sensitivity of TPG to stress and mobile water saturation are themselves controlled by permeability, generating a complex feedback. These dynamic changes in TPG during reservoir production, lead us to rename TPG as the dynamic threshold pressure gradient (DTPG). In the first part of this paper we examine the sensitivity of the DTPG to stress and mobile water saturation for cores with different permeabilities, showing that DTPG increases logarithmically with effective stress, from 0.17 MPa/m to 0.5 MPa/m for a change in effective stress from 0.6 MPa to 30.5 MPa. The DTPG also increases exponentially with mobile water saturation ( $S_m$ ), being 2.7 to 6.5 times higher at  $S_m=20\%$  compared to the value at irreducible water saturation. The sensitivity of DTPG to both variables shows a decreasing power law trend with increasing rock permeability. These combined effects generally lead to the DTPG being larger than the conventional TPG. In the second part of this paper we model the effects of using a variable DTPG in place of a constant TPG for the purpose of predicting the production loss associated with the latent pressure barrier in different heterogeneous reservoirs. When the interacting effects of effective stress, water saturation and permeability are taken into account, we find that the threshold pressure is relatively small in heterogeneous reservoirs with a distribution of increasing permeability in the gas flow direction. The constant TPG approach underestimates the production loss by 34-45% with the greatest difference occurring at low gas pressures encountered at the production well, suggesting that gas production wells should be located in areas with high permeability.

33

**Keywords:** tight gas reservoirs, permeability heterogeneity, dynamic threshold pressure gradient, stress sensitive, threshold pressure distribution, gas production loss

36

## 37 Introduction

38 Tight sandstone gas reservoirs have huge gas reserves and very significant potential for development <sup>[1-3]</sup>.  
39 Tight sandstones gas reservoirs have low or ultra-low porosity/permeability, high water saturation, strong  
40 heterogeneity, and complex gas-water seepage (flow of gas-water in rock pore-throats) <sup>[4-6]</sup>. The water film  
41 in the complex and fine pore-throats of tight gas reservoir rocks produces greater resistance to seepage <sup>[7-10]</sup>.  
42 The gas in the pore-throats needs to break through, overcoming the capillary resistance to flow from the static  
43 state <sup>[11]</sup>. Consequently, a certain displacement differential pressure is required initially to counteract this  
44 resistance, to start and then to maintain the gas flow along the pore-throat path. In tight sandstone gas  
45 reservoirs, the threshold pressure gradient (TPG) is both significant and dynamic in the sense that it depends  
46 on permeability, effective stress and water saturation <sup>[12]</sup>.

47 The pore-throat structure of the rock is the key factor controlling TPG in tight sandstone rocks <sup>[13]</sup>. The  
48 permeability of the rock is related to the complexity of the pore-throat structure <sup>[14]</sup>. Consequently, rock  
49 permeability is considered to have a significant effect on the threshold pressure in tight reservoirs <sup>[15]</sup>.  
50 Moreover, the differential pressure for gas production in tight gas reservoirs is large due to their low  
51 permeability. The drop in reservoir fluid pressure during development results in changes in the effective  
52 stress on the reservoir rock. The large variation in effective stress results in significant changes to the original  
53 small-scale pore-throat structure <sup>[16]</sup>. In addition, water saturation continues to increase during the  
54 development process, changing the water distribution in the rock's pore-throats. The variations in rock  
55 effective stress and water distribution lead to changes in the threshold pressure gradient, known as the  
56 dynamic threshold pressure gradient (DTPG) effect <sup>[17-21]</sup>. Sensitivity coefficients are used to describe how  
57 sensitive the DTPG is to changes in effective stress and mobile water saturation.

58 The dynamic nature of the TPG makes it difficult to predict the threshold pressure distribution in  
59 reservoirs at different reservoir pressures <sup>[22]</sup>. The determination of the optimal well spacing between injection  
60 and production wells lacks a basis for prediction <sup>[23]</sup>. In addition, the prediction of gas well production is  
61 complicated by the DTPG effect. Existing gas well production formulae have been established using the  
62 magnitude of the threshold pressure without taking account of its dynamic nature. The TPG is considered to  
63 be a fixed value, and this value is measured at a low effective stress <sup>[24]</sup>. The predicted threshold pressure  
64 with distance is linear according to this value, which inevitably leads to an underestimated calculated gas  
65 production loss. Consequently, the predicted gas production is overestimated, resulting in actual production

66 deviating from expected development schedule.

67 The TPG is affected by rock permeability, especially in the case of tight reservoirs with strong permeability  
68 heterogeneity. The calculation of threshold pressure distribution and the prediction of gas production are  
69 more complicated, as is the effect of DTPG. Consequently, it is important to understand the distribution of  
70 DTPG in tight gas reservoirs<sup>[25]</sup>. Such understanding can facilitate the design of the appropriate development  
71 parameters and well pattern layout to reduce the gas production loss caused by DTPG.

72 The TPG of tight sandstones at different permeabilities and conditions of water saturation have been  
73 tested on cores in previous studies<sup>[11-13, 22]</sup>. Small rock permeability values are considered to be associated  
74 with small pore-throat structures. This agrees with the relevant theoretical petrophysics and with results from  
75 nanometer scale 3D scanning of shales<sup>[26-30]</sup>. Pore-throats with small radii produce large capillary resistance.  
76 In addition, more fluid flow channels are blocked with the increased water saturation. Consequently, the  
77 combination of low permeabilities and high mobile water saturations result in tight reservoirs with large  
78 values of TPG<sup>[31-32]</sup>. The sensitivity of TPG to mobile water saturation has been tested in our previous studies  
79<sup>[22]</sup>, showing that mobile water has a greater effect on TPG than irreducible water<sup>[11]</sup>. Moreover, the TPG  
80 values increase with effective stress<sup>[33]</sup>, which is attributed to increased capillary resistance due to a decrease  
81 in pore-throat size<sup>[18, 34]</sup>. This is analogous to the stress sensitivity of permeability<sup>[22]</sup>.

82 The sensitivity of DTPG to stress and mobile water is closely related to permeability and its  
83 heterogeneity. However, published studies have not taken into account the heterogenous nature of  
84 permeability, the sensitivity of DTPG to effective stress and mobile water saturation and the effects of  
85 changing permeabilities, despite the distribution of DTPG being closely related to permeability heterogeneity  
86 as gas production progresses. Calculations based on our experimental tests reported in this work lead us to  
87 conclude that, there are large differences in the DTPG distributions in reservoirs with the same average  
88 permeability but different heterogeneity distributions under the same stress conditions. Development  
89 parameters and well deployment for different permeability heterogeneity distributions in tight reservoirs can  
90 then be established to reduce the threshold pressure.

91 Unfortunately, the distribution of DTPG in tight reservoirs with permeability heterogeneity has not  
92 previously been studied. Research on the threshold pressure variation with distance from injection and  
93 production wells, and the gas production loss due to DTPG in the permeability-heterogeneous tight reservoir  
94 has also not been reported.

95 In this paper, we study the sensitivity of rock DTPG to effective stress and mobile water saturation in

96 heterogeneous tight gas reservoirs, and ultimately predict the distribution of DTPG within such reservoirs.  
97 Measurements of the DTPG of tight sandstone cores with different permeabilities have been carried out by  
98 using the improved bubble method [22]. The variation in characteristics of the DTPG at different effective  
99 stress values and saturations of mobile water has also been studied. The impact of rock permeability on  
100 effective stress sensitivity coefficient and mobile water sensitivity coefficient of DTPG has been analyzed  
101 quantitatively. The threshold pressure distribution in the heterogeneous reservoir has then been calculated  
102 using the DTPG. In particular, the influence of the distribution of the permeability heterogeneity and  
103 reservoir pressures on the threshold pressure distribution are reported, and gas production loss related to these  
104 issues is discussed. The results with DTPG were compared with those corresponding to the conventional  
105 fixed threshold pressure gradient (FTPG). The results provide both the base data and theoretical basis that  
106 support the prediction of threshold pressure in tight gas reservoirs and calculation of gas production in this  
107 type of reservoirs.

108

## 109 **Methodology**

### 110 **Materials**

111 Nine sandstone cores (numbered Y1-Y6 and C1-C3) were chosen from a target tight reservoir at a depth of  
112 3000-3100 m. The cores C1-C3 were divided into two equal parts, each 3.5 cm long (Table 1). The reservoir  
113 temperature is  $82\pm 1.8^{\circ}\text{C}$ , the rock porosity varied from 3% to 13%, with an arithmetic mean of 8.1%, while  
114 the permeability varied between  $0.02\times 10^{-3}\ \mu\text{m}^2$  and  $0.2\times 10^{-3}\ \mu\text{m}^2$ , with an arithmetic mean of  $0.08\times 10^{-3}\ \mu\text{m}^2$   
115 and a geometric mean of  $0.09\times 10^{-3}\ \mu\text{m}^2$ . Cores Y1-Y6 were cut so that all cores were 7 cm in length (Table  
116 1). The samples were studied by X-ray diffraction for elemental and mineral composition. The average total  
117 content of quartz and feldspar of these samples is greater than 75%.

118 The brine used in all experimental tests was prepared to match known formation water data for the field  
119 (Table 2). Cores were immersed in brine and aged for 24 hours, to reduce any differences in the wettability  
120 of mineral surfaces in different cores as much as possible. This is important in order to reduce the effect of  
121 wettability differences on the distribution of gas-water transport through the cores during tests, so that the  
122 effect of other parameters can be more easily ascertained [35]. Pure humidified  $\text{CH}_4$  were used to represent the

123 gas of reservoir in the experiments.

124  
125

Table 1. Basic parameters of the core samples.

No.	$L$ (cm)	$D$ (cm)	$\phi$ (%)	$k$ ( $10^{-3} \mu\text{m}^2$ )	$S_{wi}$ (%)
Y1	7.093	2.535	5.35	0.0258	48.5
Y2	7.117	2.527	8.843	0.0346	50.2
Y3	7.081	2.521	7.975	0.0459	45.7
Y4	7.066	2.534	7.737	0.0781	44.8
Y5	7.121	2.532	8.506	0.1158	40.6
Y6	7.216	2.524	9.008	0.1224	38.9
C1-1	3.652	2.521	6.868	0.0251	
C2-1	3.493	2.522	8.102	0.0679	47.9
C3-1	3.817	2.526	9.642	0.1295	
C1-2	3.611	2.521	6.868	0.0248	
C2-2	3.473	2.522	8.102	0.0684	48.5
C3-2	3.784	2.526	9.642	0.1253	

126 *Note.*  $L$  core length,  $D$  core diameter,  $\phi$  porosity,  $k$  Klinkenberg permeability,  $S_{wi}$   
127 irreducible water saturation

128  
129

Table 2. Physicochemical properties of the reservoir brine measured at 20°C.

Item	Value
Density ( $\text{g}/\text{cm}^3$ )	1.031
pH	6.74
$\text{K}^+$ (mg/L)	2318
$\text{Na}^+$ (mg/L)	1148
$\text{Ca}^{2+}$ (mg/L)	4314
$\text{Mg}^{2+}$ (mg/L)	390
$\text{Cl}^-$ (mg/L)	22344
$\text{HCO}_3^-$ (mg/L)	1148
$\text{SO}_4^{2-}$ (mg/L)	1809
TDS (mg/L)	41614

130

TDS = Total dissolved solids

## 131 Threshold pressure test method

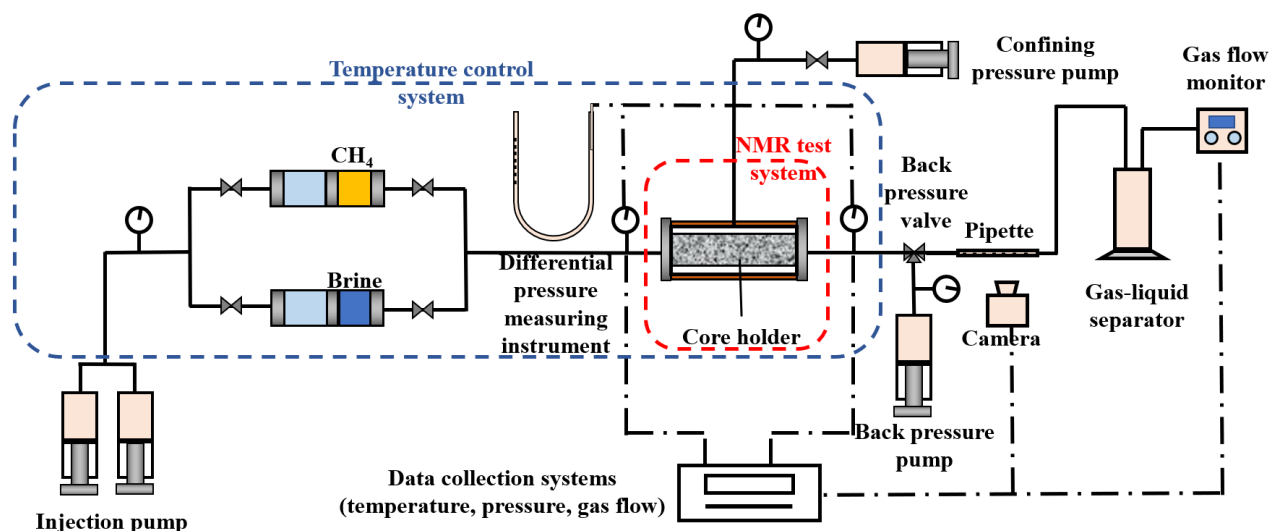
132 The threshold pressure values were measured by an improved bubble method<sup>[22]</sup>. First, a small displacement  
133 differential pressure is applied to the core by injecting  $\text{CH}_4$ . A thin pipette containing air bubbles in dyed  
134 water is connected to the outlet end of the core. The displacement differential pressure is then increased  
135 continuously. The gas starts to flow in the core when the differential pressure overcomes the capillary  
136 resistance, which causes the bubbles to move. At this point, the differential pressure between the two ends of  
137 the core is the minimum threshold pressure for which the two phases of gas-water can flow<sup>[36]</sup>. The bubbles

138 in the thin pipette are monitored by a camera and a computer. Once any movement of bubbles is detected by  
 139 the camera and the computer, the computer immediately records the pressure data, improving the accuracy  
 140 of the measurement. During DTPG tests, the differential pressure is monitored by a dynamic differential  
 141 pressure gauge. This device can continuously monitor the dynamic change of differential pressure on the  
 142 order of  $10^{-6}$  MPa while the system working pressure is over 50 MPa.

### 143 Test equipment and procedures

144 The main experimental devices are the core displacement system and the matching nuclear magnetic  
 145 resonance (NMR) test system, as shown in Figure 1.

146  
 147



148  
 149  
 150

Figure 1. TPG test experimental device.

151 The measurement steps are as follows,

152 (1) The fluid transfer vessels were filled with CH<sub>4</sub> and brine together with the core holder were placed in the  
 153 temperature controlled chamber. The chamber temperature was set to 82°C and left for 24 hours for the  
 154 temperature to equilibrate in all parts of the heated equipment.

155 (2) The brine saturated core was placed in the core holder with confining pressure of 31 MPa. The brine in  
 156 the core was then gradually displaced by CH<sub>4</sub> injection. The core holder was placed in the NMR equipment  
 157 for NMR scanning. The brine distribution was monitored, and the corresponding brine saturation was  
 158 calculated. The brine in the core was displaced by CH<sub>4</sub> injection until the water saturation reached specified

159 pre-defined value.

160 (3) The pressure at the outlet end of the core was stabilized at 30.4 MPa by the back-pressure pump and the  
161 back-pressure valve at irreducible water saturation ( $S_{wi}$ ). The differential pressure was then increased from a  
162 starting value of  $1 \times 10^{-3}$  MPa in increments of  $1 \times 10^{-3}$  MPa by injecting CH<sub>4</sub>. At each pressure value, the  
163 pressure was stabilized for 3 hours until the bubble movement in the pipette was recognized. The TPG at this  
164 back-pressure was recorded. Otherwise, the differential pressure was gradually increased until the bubble  
165 moved. The back-pressure was set to the next value in a total of 11 other back-pressure values in the range  
166 of 0.5-30.4 MPa, and the TPG values at different pressures were measured, respectively.

167 (4) Steps (1)-(3) were repeated to test TPG at different mobile water saturations ( $S_m$ ) at 30.4 MPa back-  
168 pressure (in this paper, the irreducible water saturation ( $S_{wi}$ ) and the water saturation ( $S_w$ ) of nominally  $S_{wi}+8\%$ ,  
169  $S_{wi}+15\%$ , and  $S_{wi}+20\%$ , respectively, in total 4 saturation values, and  $S_m=S_w-S_{wi}$ ). The core that was in the  
170 holder was then replaced, and tests were performed on the other cores.

171 After the tests, the cores were tested by NMR to measure their water saturation. If the difference in brine  
172 saturation was less than 2%, this group experimental data was considered to be reliable. Otherwise, the  
173 experimental differential pressure and the TPG value was retested.

## 174 Results and discussion

### 175 Sensitivity of DTPG to effective stress

176 The DTPG values of the cores with different effective stresses ( $P_{eff}$ ) at irreducible water saturation are shown  
177 in Figure 2, where the abscissa is logarithmic. The core outlet was connected to the atmosphere in  
178 conventional threshold pressure tests. The pressure at the outlet was 0.1 MPa, and the corresponding effective  
179 stress was a small fixed value. In fact, the DTPG- $P_{eff}$  curve shows an increasing trend, where the increase is  
180 rapid for  $P_{eff}<5$  MPa, with a variation amplitude of 0.1-0.3 MPa/m, and the increase becomes slower for  
181  $P_{eff}>5$  MPa. Consequently, the TPG values tested in conventional threshold pressure tests are relatively small  
182 and are also below those encountered during the development of reservoirs.

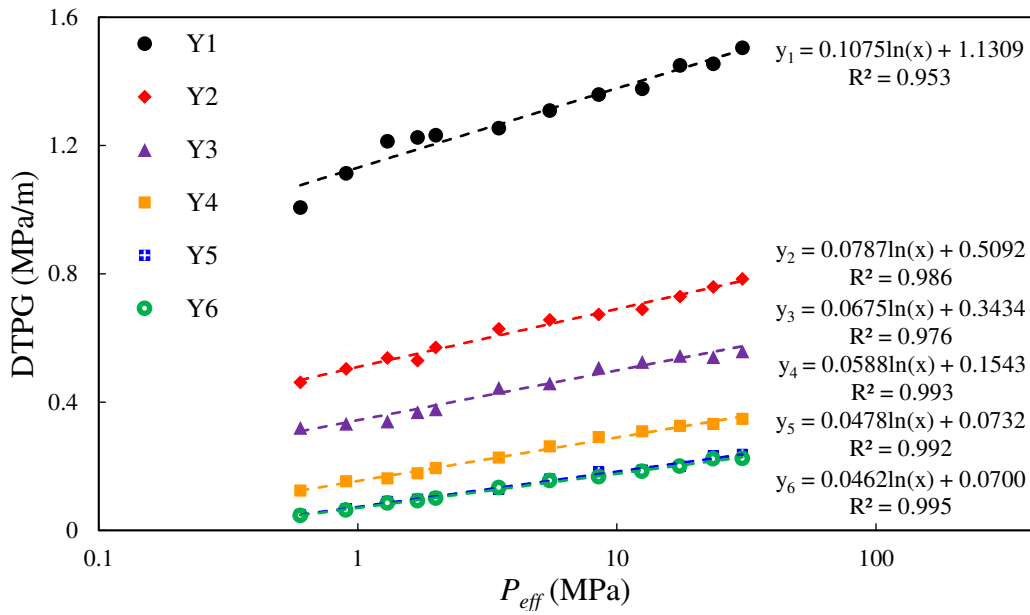
183 The total amplitude of the DTPG varies logarithmically between 0.17 and 0.5 MPa/m for variations of  
184  $P_{eff}$  between 0.6 and 30.5 MPa. The DTPG- $P_{eff}$  data are well-fitted by a relationship of the following form,

$$185 \quad \Delta P_{thresh} = \lambda \ln(P_{eff}) + a \quad (1)$$

186 where  $\Delta P_{thresh}$  is TPG (MPa/m),  $P_{eff}$  is the effective stress (MPa), and  $\lambda$  and  $a$  are fitting coefficients (MPa/m).

187 The coefficient  $\lambda$  is the slope of the line in Figure 2, a key parameter controlling the increase of the  
 188 DTPG- $P_{eff}$  curve, called as the DTPG stress sensitivity coefficient. The coefficient  $\lambda$  is used to describe the  
 189 sensitivity of the DTPG to changes in  $P_{eff}$ . The coefficient  $a$  determines the average level of the DPTG values,  
 190 corresponding to the upper (DPTG<sub>max</sub>) and lower (DPTG<sub>min</sub>) limits of DPTG, and  $\lambda$  determines the variation  
 191 range of DPTG [5].

192



193

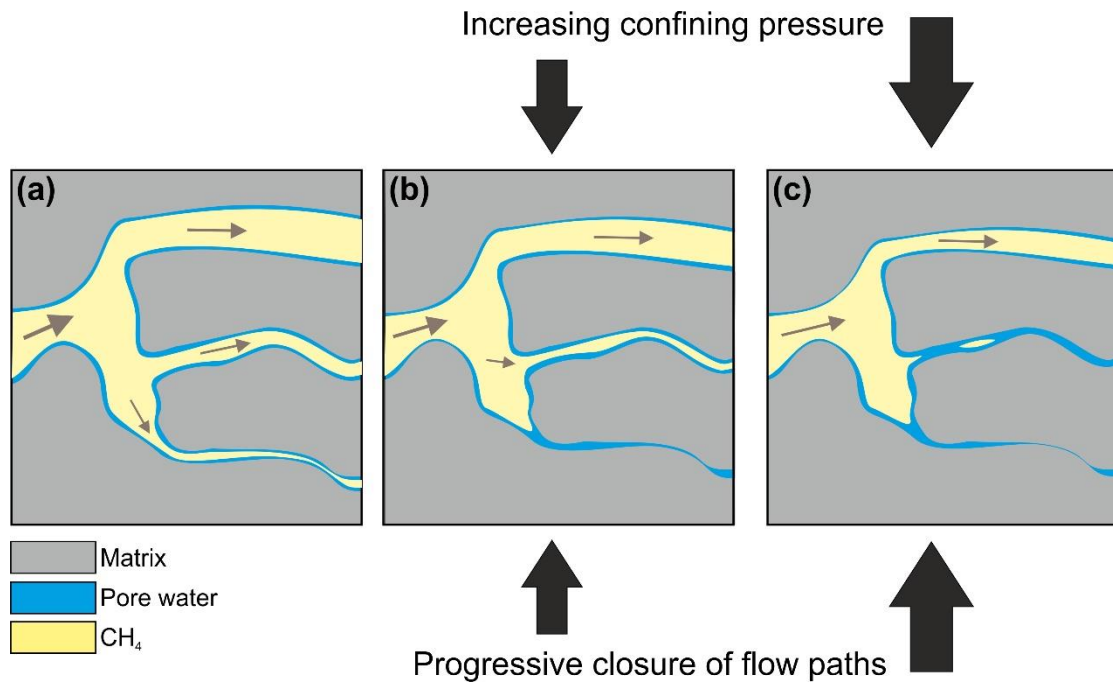
194

195 Figure 2. DTPG and effective stress pressure ( $P_{eff}$ ) of cores at irreducible water saturation ( $S_{wi}$ ).

196

197 The mechanism of rock DPTG stress sensitivity is considered to be similar to that of rock permeability stress  
 198 sensitivity [37]. The only difference is in the interpretation of the flow process. In the case of permeability, it  
 199 is assumed that a gas flow is taking place at a given differential gas pressure. Increasing the confining pressure,  
 200 as shown in Figure 3, reduces the aperture of flow paths, the number of flow paths available for flow, and  
 201 their connectivity. Closure of flow paths due to increasing overburden pressure reduces all three of these  
 202 controls on permeability. By contrast DPTG assumes that flow is not taking place and measures the pressure  
 203 difference required to start flow. Figure 3a shows that for relatively low confining pressures flow is already  
 204 taking place, indicating that the local DTPG is exceeded in all three channels. As confining pressure increases  
 205 (Figure 3b), flow is taking place at a differential pressure which is greater than the local DTPG for the top  
 206 two channels, but has not exceeded the capillary pressure allowing flow in the bottom channel, leaving the

207 channel blocked by a water slug <sup>[38]</sup>. As overburden pressure increases further (Figure 3c), flow is taking  
 208 place at a differential pressure which is greater than the local DTPG for only the top channel, while the bottom  
 209 two channels do not flow because the differential pressure has not exceeded the local DTPG for these  
 210 channels. Consequently, the control of channel aperture imposed by the overburden pressure controls both  
 211 the DTPG and the fluid permeability <sup>[39]</sup>.  
 212  
 213

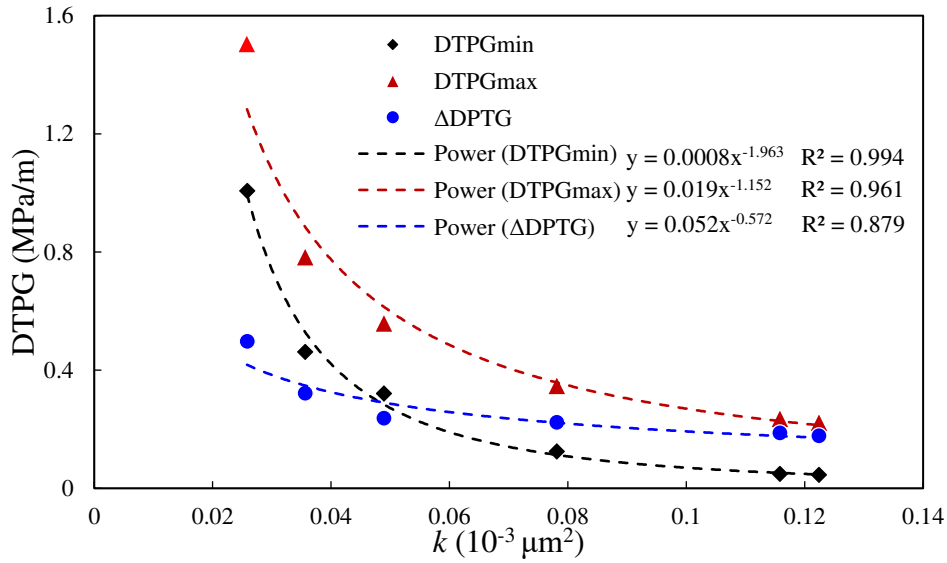


214  
 215  
 216 Figure 3. Schematic diagram of the mechanism of DPTG stress sensitivity and permeability stress  
 217 sensitivity.  
 218

219 We define  $DTPG_{min}$  as the DTPG value at minimum effective stress of the rock, and  $DTPG_{max}$  as the  
 220 DTPG value at the maximum effective stress of the rock, as well as the difference between the two,  $\Delta DTPG =$   
 221  $DTPG_{max} - DTPG_{min}$ . Figure 4 shows that all three of these parameters decrease non-linearly as permeability  
 222 increases. The average pore-throat radius is small in low permeability rock, the capillary resistance formed  
 223 by the water slug is large, and the TPG value is large. The rate of decrease of the DTPG values with increasing  
 224 permeability is greater for rocks with smaller permeabilities. This is because the complexity of the pore-  
 225 throat structure increases exponentially with the decrease of the permeability value at smaller permeability  
 226 values <sup>[40]</sup>. The TPG is more sensitive to the variation of the permeability value in lower permeability rocks.  
 227 The variation range of  $\Delta DTPG$  also decreases with increasing permeability, indicating that changes in DTPG

228 with effective stress become much smaller as permeability increases.

229



230

231

232 Figure 4. The variations of DTPG<sub>max</sub> and DTPG<sub>min</sub> versus core permeability ( $k$ ).

233 (DTPG<sub>max</sub>, DTPG value at minimum effective stress of rock; DTPG<sub>min</sub>, DTPG value at maximum effective  
 234 stress of rock;  $\Delta$ DPTG= DTPG<sub>max</sub>- DTPG<sub>min</sub>.)

235

236 There are differences in the trend of DTPG- $P_{eff}$  for cores with different permeability, as shown in Figure

237 2. Large permeabilities correspond to small DTPG values, and the slope of the DTPG- $\log(P_{eff})$  curve is

238 smaller at higher permeabilities, implying that rocks with larger permeabilities exhibit weaker dependence

239 on effective stress.

240 The  $\lambda$ - $k$  and  $a$ - $k$  curves are shown in Figure 5. Both the  $\lambda$ - $k$  curve and  $a$ - $k$  curve show downward trends.

241 Smaller permeability samples exhibit larger  $\lambda$  and  $a$  coefficients, implying that small permeability samples

242 have both large DTPG values and larger sensitivity to changing effective stress. In particular,  $\lambda$  and  $a$  are

243 more sensitive to permeability variations at low permeabilities ( $<0.06 \times 10^{-3} \mu\text{m}^2$ ). This is similar to the

244 sensitivity of DTPG to effective stress, because rocks with low permeability have small pore-throats and

245 complex pore-throat structures. A small effective stress variation causes a large change in pore-throat

246 structure and also results in a large change in the water distribution<sup>[41]</sup>. In this case, the DTPG shows a strong

247 sensitivity to the effective stress.

248

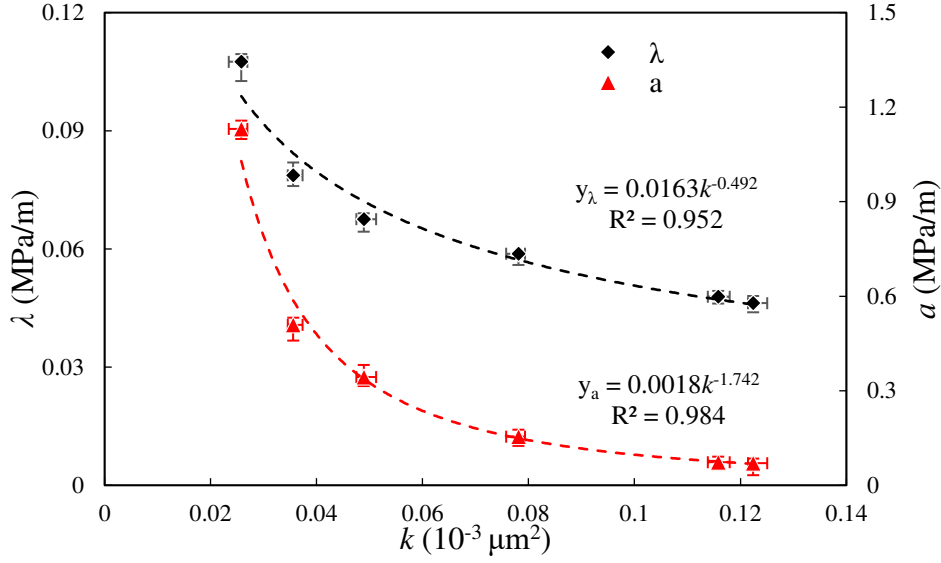


Figure 5. Rock DTPG stress sensitivity coefficient ( $\lambda$ ,  $a$ ) versus core permeability ( $k$ ).

249  
250  
251  
252

### 253 Sensitivity of DTPG to mobile water

254 Tight gas reservoirs always have high-water saturations due to the small and complex pore-throat structure  
 255 [3-4], which results in relatively large values of threshold pressure. Moreover, the water saturation continues  
 256 to rise during production, which leads directly to a large variation in the water distribution in the pore-throats  
 257 of the rock [42]. If we consider the scenario illustrated by Figure 3 and then imagine that the water saturation  
 258 increases, the result will be that there is no change to the pathways that are already blocked, but some of the  
 259 open pathways may also become blocked by a water slug. The middle channel in Figure 3b is at particular  
 260 risk of this happening if the local water saturation increases. While this scenario is valid for all overburden  
 261 pressures, it is more likely to pose a threat at higher overburden pressures where many of the pathways for  
 262 flow are already small if not already blocked and the DTPG is already high. Consequently, water saturation  
 263 is also a key factor controlling the DTPG values.

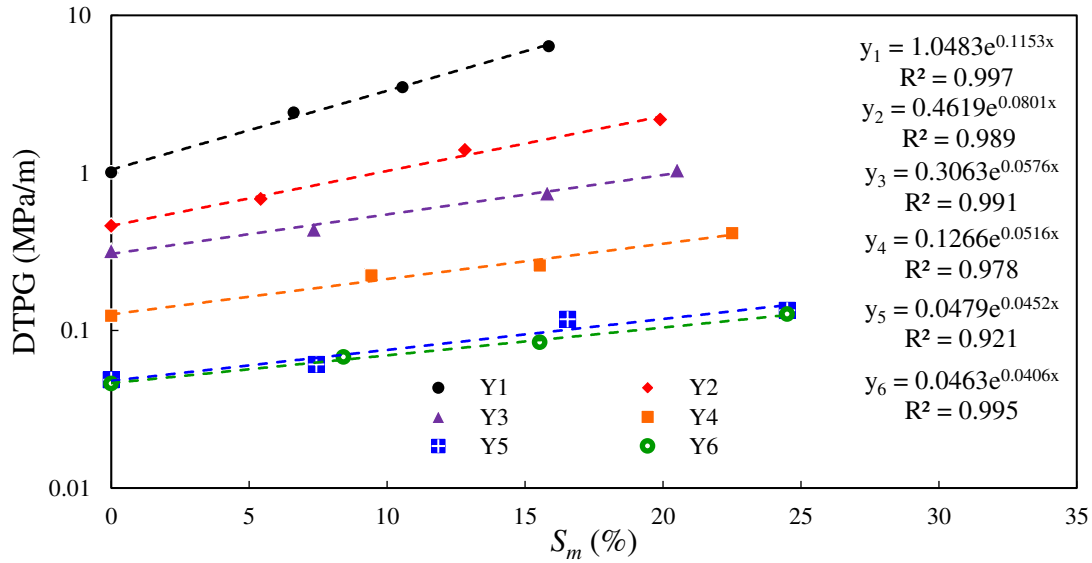
264 The relationship between the mobile water saturation ( $S_m$ ) and DTPG at  $P_{eff}$  of 0.6 MPa is shown in  
 265 Figure 6. The DTPG of the cores are 2.7 to 6.5 times the initial value from  $S_{wi}$  to an  $S_m$  of 25%. The DTPG-  
 266  $S_m$  relationship shows an exponential increase, exemplified by linear behavior when plotted on semi-  
 267 logarithmic axes, as here. The relationship is given by,

$$268 \quad \Delta P_{thresh} = be^{\eta S_m} \quad (2)$$

269 where  $\Delta P_{thresh}$  is the TPG (MPa/m),  $S_m$  is the mobile water saturation (%), and  $\eta$  (in units of  $\%^{-1}$ ) and  $b$

270 (MPa/m) are fitting coefficients.

271 The coefficient  $\eta$  is the slope of the line, a key parameter controlling the increase of the value of DTPG  
 272 with water saturation. This parameter is defined as the DTPG mobile water sensitivity coefficient [22]. The  
 273 coefficient  $\eta$  is used to describe the sensitivity of the DTPG to changes in saturation of mobile water. The  
 274 parameter  $\eta$  determines how quickly the curve increases, and the coefficient  $b$  is the DTPG value at  $S_{wi}$ .  
 275



276  
 277  
 278 Figure 6. DTPG and mobile water saturation ( $S_m$ ) of cores at 0.6 MPa effective stress pressure ( $P_{eff}$ ).  
 279

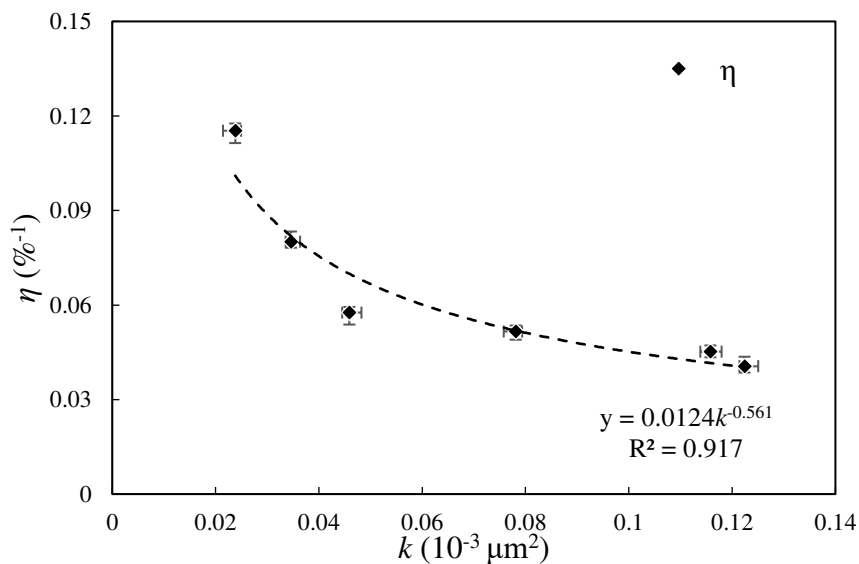
280 Water is the wetting phase in the rock pores. The irreducible water generally covers the pore walls in  
 281 the form of water film or fills the smallest pore throats. Gas is the non-wetting phase and is distributed in the  
 282 center of the relatively larger pore-throats in the flow channel. Water slugs cause relatively little blockage of  
 283 such larger pore-throat diameter gas flow paths. Contemporaneously, there is free-flowing mobile water in  
 284 pore-throats at higher saturations than  $S_{wi}$ . The thickness of the water film on the pore wall increases as water  
 285 saturation increases. The mobile water fills the pore-throats that were not originally occupied by the  
 286 irreducible water, resulting in blockage of the gas transport path for a large range of pore-throat diameters,  
 287 and the DTPG consequently increases. As  $S_m$  continues to increase, some of the relatively larger pore-throats  
 288 become filled with water [43], extending the range of pore-throat sizes [43] occupied by water slugs to encompass  
 289 larger pore-throats as well as the smaller pore-throats which were previously not occupied by water slugs.  
 290 Hence, the total length of flow channel occupied by water slugs increases, which leads to a significantly  
 291 increase of DTPG. Consequently, the DTPG increases exponentially with  $S_m$ .

292 Compared with the logarithmic increasing trend of DTPG- $P_{eff}$ , the exponential increasing trend of DTPG

293 as a function of  $S_m$  indicates that the sensitivity of DTPG to mobile water is stronger than that of effective  
 294 stress. The increase in water saturation is the direct cause of the existence of the water slug in the pore-throats,  
 295 which directly produces the gas-water two-phase fluid transport resistance. By contrast, increases in effective  
 296 stress mainly affects the DTPG by reducing the pore-throat radius when the pores contain water, and plays a  
 297 more indirect role. The DTPG effect caused by the direct variation of water distribution is consequently more  
 298 significant than the indirect effect of the pore-throat size change caused by stress sensitivity.

299 When the water saturation of cores with different permeability increases by the same value, the  
 300 distribution of the increased mobile water in the pore-throat of different cores is different due to the difference  
 301 in the complexity of the pore-throat structure, resulting in different impact on the DTPG. The pore-throat  
 302 radius of low permeability cores is smaller and more complex than that of rocks with higher permeabilities.  
 303 The increasing mobile water saturation immediately produces a significant increase in the DTPG in low  
 304 permeability rocks. The overall DTPG- $S_m$  trend is steep and the sensitivity of DPTG to mobile water is  
 305 affected by rock permeability. The  $\eta$ - $k$  curve is shown in Figure 7. The  $\eta$ - $k$  curve also shows a decreasing  
 306 power law relationship. The sensitivity coefficient  $\eta$  decreases rapidly with the permeability at low  
 307 permeability values, while the variation of  $k$  has relatively little effect on  $\eta$  at large permeability values. That  
 308 is, when the permeability is small, the sensitivity of  $\eta$  to  $k$  is strong, and when the permeability is large the  
 309 sensitivity of  $\eta$  to  $k$  is weak.

310



311

312

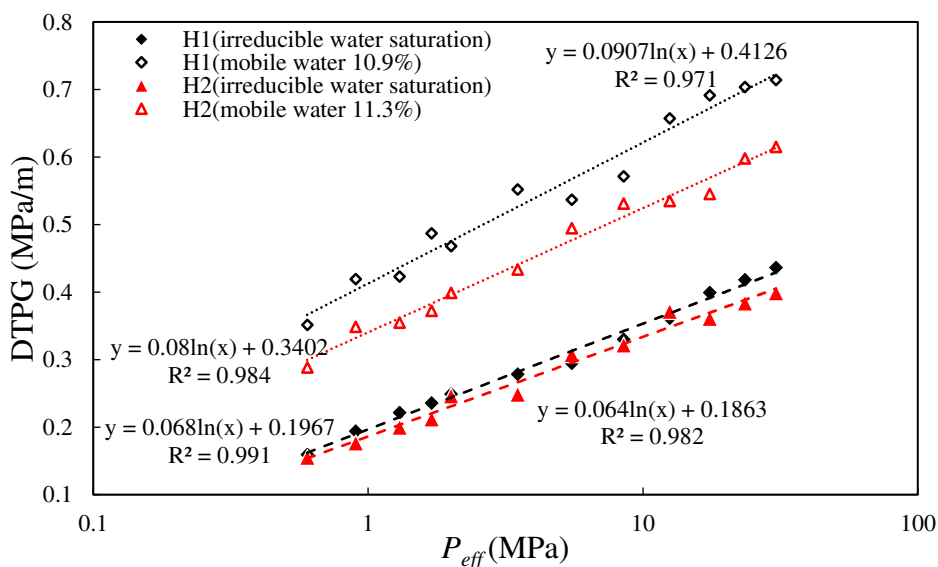
313

314

Figure 7. Rock DTPG mobile water sensitivity coefficient ( $\eta$ ) versus core permeability ( $k$ ).

315 DTPG and permeability heterogeneity

316 Strong heterogeneity is another major feature of tight gas reservoirs [44]. Cores with different permeability  
 317 have different pore-throat structures and differences in the water distribution in pore-throats [45]. The  
 318 heterogeneity resulting from the deliberate combination of short cores to form composite cores with different  
 319 permeability also affects the DTPG. The effect of heterogeneity on DTPG and its controlling influences has  
 320 been studied by carrying out measurements on composite cores that are composed of three short cores with  
 321 different properties. The composite core H1 is composed of short cores C1-1, C2-1, C3-1, with permeability  
 322 decreasing progressively in the flow direction. The composite core H2 is composed of short cores C1-2, C2-  
 323 2, C3-2, and has progressively increasing permeability in the flow direction (see Table 1). Figure 8 shows  
 324 the DTPG- $P_{eff}$  relationships for the composite cores H1 and H2 at different water saturation conditions.  
 325

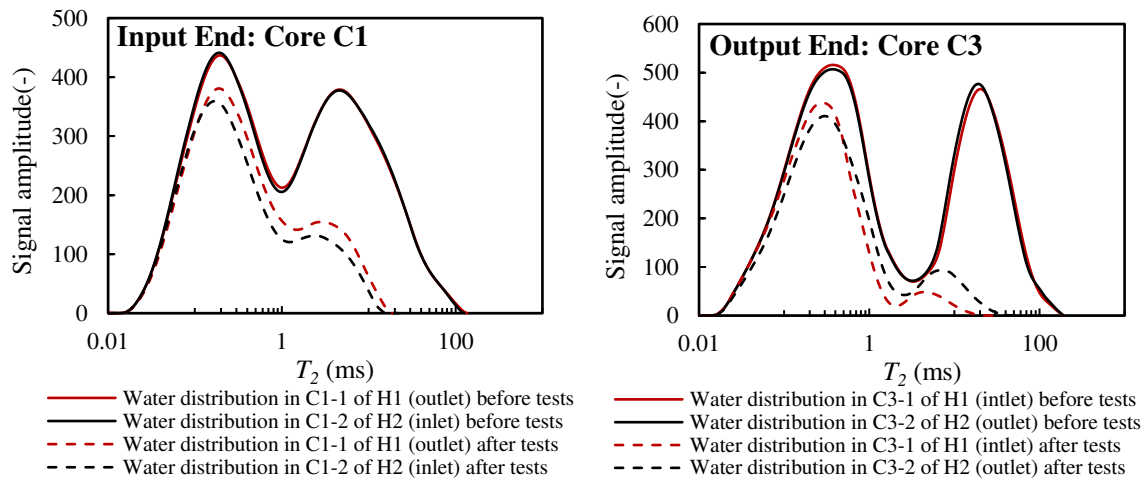


326  
 327  
 328 Figure 8. DTPG versus effective stress ( $P_{eff}$ ) of composite cores.  
 329

330 Similarly to the previously tested cores (Figure 2), the DTPG- $P_{eff}$  curves of both composite cores H1  
 331 and H2 also show a logarithmic increasing trend. Moreover, the DTPG- $P_{eff}$  curves of cores H1 and H2 show  
 332 a large difference at about 11%  $S_m$ . That is, the DTPG values and the effective stress sensitivity are different  
 333 under different fluid flow directions in the heterogeneous core. Clearly, H1 has higher DTPG values and is  
 334 more sensitive to changes in effective stress. This may be due to the difference in the distribution of mobile  
 335 water in cores.

336 Figure 9 shows the NMR  $T_2$  distributions before and after the DTPG tests for the inlet and outlet cores

337 for each composite arrangement. The inlet of core H1 is C3-1 (high permeability core), and the outlet is C1-1  
 338 1 (low permeability core). The inlet end of core H2 is C1-2 (low permeability core), and the outlet is C3-2  
 339 (high permeability core). The purpose of this figure is to ascertain what the effect of carrying out the gas-  
 340 flooding tests are, and whether the change in water saturation and mobility is affected by the permeability  
 341 and/or position of the core in the composite in order to determine whether the mobility of the water depends  
 342 on the permeability heterogeneity of the composite cores.  
 343



344  
 345 Figure 9. The water distribution in the inlet and outlet of the cores H1 and H2 before and after DTPG tests.  
 346

347 The  $T_2$  distributions in all four of the initially saturated cores (i.e., before the DTPG tests) are bimodal,  
 348 indicating that (i) the cores have been chosen well to have very similar microstructural characteristics despite  
 349 having different permeabilities, and (ii) the cores contain both capillary-bound water, represented by the  
 350 peaks draped around 0.2-0.4 ms, and mobile water, represented by the peaks centered around higher values  
 351 of  $T_2$ . It should be noted that none of the samples conform to the standard, and often erroneous 33 ms cut-off  
 352 that is often applied blindly in the oil and gas industry. The NMR  $T_2$  distributions measured after the DTPG  
 353 tests in each case show that most of the mobile water gas been produced from the cores, together with a  
 354 significant amount of capillary bound water. Water production is marginally greater for cores placed at the  
 355 outlet.

356 In the core H1, the permeability decreases along the direction of the displacement differential pressure,  
 357 and more mobile water is distributed in the small permeability core near the outlet<sup>[46]</sup>. The DTPG values are  
 358 larger for cores with smaller permeabilities, as is their sensitivity to changes in effective stress and mobile

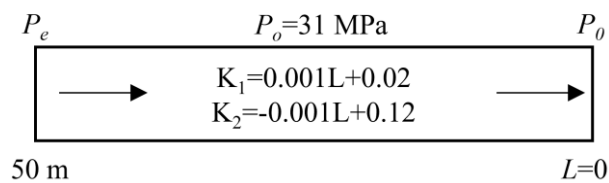
359 water as shown in Figure 5 and Figure 7. In the core H2, more mobile water is distributed in the large  
 360 permeability core near the outlet, the value of DTPG is small and the sensitivity is weak. At irreducible water  
 361 saturation, the water distribution in cores with different permeability is relatively more uniform. There is a  
 362 difference in DTPG between H1 and H2 at irreducible water saturation, but the difference is small. That  
 363 difference becomes more significant as water saturation increases. Consequently, the direction of reservoir  
 364 flow is important from the point of view of DTPG as well as the more conventional considerations of  
 365 permeability and breakthrough. Hence, the choice of the relative location of injection and production wells  
 366 can effectively reduce the TPG during the development of heterogeneous tight gas reservoirs.

367

### 368 Threshold pressure distribution

369 The core test results represent the parameters of a point in the reservoir. The test results cannot characterize  
 370 the distribution of the TPG in a heterogeneous reservoir at the reservoir scale. Figure 10 shows a schematic  
 371 diagram of a one-dimensional heterogeneous tight gas reservoir with a length of 50 m at irreducible water  
 372 saturation. The overburden pressure ( $P_o$ ) is 31 MPa, and there are two possible permeability distributions, (i)  
 373  $K_1$ , where the permeability of the reservoir decreases gradually from left to right ( $0.12 \times 10^{-3} \mu\text{m}^2$  to  $0.02 \times 10^{-3}$   
 374  $\mu\text{m}^2$ ), and (ii)  $K_2$ , where the reservoir permeability increases gradually from left to right ( $0.02 \times 10^{-3} \mu\text{m}^2$  to  
 375  $0.12 \times 10^{-3} \mu\text{m}^2$ ).

376



377

378

379 Figure 10. Schematic of one-dimensional linear reservoir with permeability heterogeneity.

380 The black arrow represents the flow direction,  $L=0$  m represents the production end,  $P_o$  is the pressure at  
 381 production end,  $L=50$  m represents the reservoir edge,  $P_e$  is the pressure at reservoir edge,  $P_o$  is the  
 382 overburden pressure,  $K_1$  represents a decreasing permeability distribution mode along the flow direction,  
 383 and  $K_2$  represents an increasing permeability distribution mode along the flow direction.

384

385 When the differential pressure gradient is larger than the TPG in the reservoir, then the fluid starts to  
 386 flow [22], that is,

$$\begin{aligned}
 &v = 0 \\
 &v = \frac{k_g}{\mu} \left( \frac{dP}{dL} - \Delta P_{thresh} \right)
 \end{aligned}
 \left\{
 \begin{aligned}
 &\frac{dP}{dL} \leq \Delta P_{thresh} \\
 &\frac{dP}{dL} > \Delta P_{thresh}
 \end{aligned}
 \right.
 \quad (3)$$

390 where  $v$  is gas flow rate (m/s),  $dP/dL$  is the displacement pressure gradient (MPa/m),  $P$  is the pore fluid  
 391 pressure at any point in the reservoir (MPa),  $L$  is the distance from the production well (m),  $\Delta P_{thresh}$  is the  
 392 TPG (MPa/m),  $k_g$  is the gas permeability ( $10^{-3} \mu\text{m}^2$ ), and  $\mu$  is the gas viscosity (mPa·s).

393 The conventional TPG is considered to have a fixed value, the threshold pressure increases linearly in  
 394 the reservoir with the distance ( $L$ ), and the slope of the straight line is the fixed threshold pressure gradient  
 395 (FTPG). According to the test results in this paper, the TPG in the reservoir is not a fixed value during the  
 396 production process. It is expected that the relationship between the threshold pressure and distance is not  
 397 linear. Moreover, the required cumulative displacement differential pressure increases to overcome the  
 398 threshold pressure. The corresponding  $P$  at any position in reservoir also increases when the pressure at the  
 399 production end is set at a higher value, while the  $P_{eff}$  decreases, the DTPG decreases. When the  $P_e$  is increased  
 400 continuously to overcome the threshold pressure, the threshold pressure decreases. The value of  $P_e$  and  
 401 threshold pressure are coupled with each other and change dynamically [22].

402 In the one-dimensional heterogeneous tight gas reservoir, when the value of the pressure  $P_0$  at  $L=0$  m is  
 403 determined (which can be considered as the pressure at the production well), there is a minimum  $P_e$  value  
 404 ( $P_{emin}$ ) at the reservoir edge ( $L=50$  m), which is just large enough for the gas to start flowing. Hence, the value  
 405 of  $P_{emin}$  is the minimum pressure when gas starts flowing. The threshold pressure of the gas-water two-phase  
 406 transport at  $P_{emin}$  in reservoirs is the maximum, which is  $P_{emin} - P_0$ . The displacement pressure gradient is just  
 407 larger than the DTPG at any position in reservoir [11].

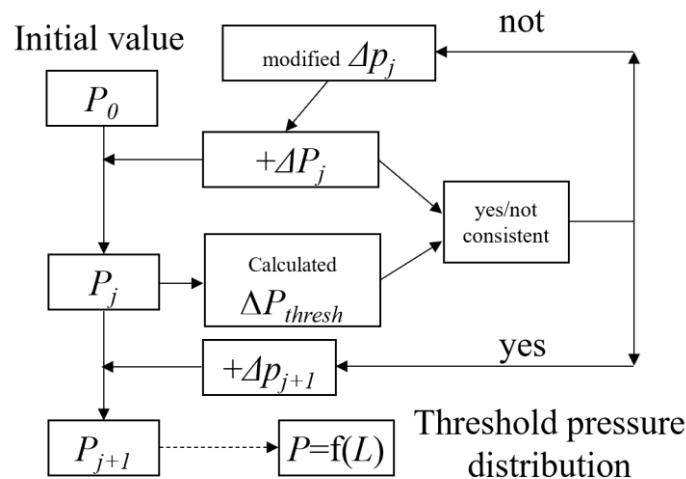
$$\frac{dP}{dL} = \Delta P_{thresh} \quad (4)$$

409 According to the test results of DTPG stress sensitivity at irreducible water saturation of tight gas  
 410 reservoir rock that we have reported previously in this paper, the DTPG in the reservoir is,

$$\left\{
 \begin{aligned}
 &\Delta P_{thresh} = \lambda \ln(P_{eff}) + a \\
 &\lambda = 0.0163k^{-0.492} \\
 &a = 0.0018 k^{-1.742}
 \end{aligned}
 \right.$$

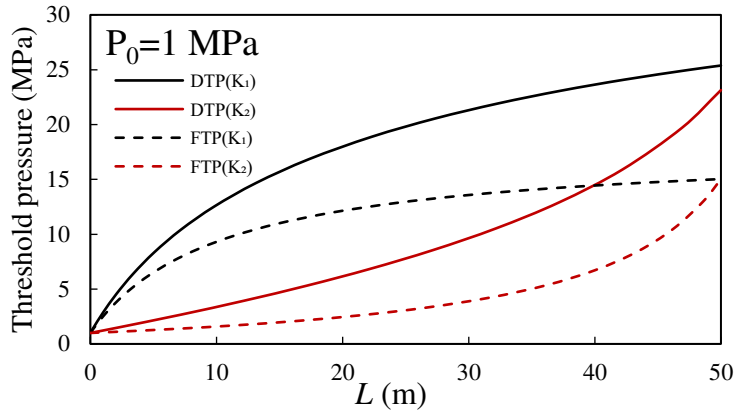
415  $k_1 = 0.001L + 0.02$   
 416  $k_2 = -0.001L + 0.12$   
 417  $P_{eff} = P_o - P$   
 418 (5)

419 Combining Eqs. (4) and (5), the iterative trial calculation can be performed by using MATLAB tools,  
 420 and the algorithm is shown in Figure 11. In this paper we set the initial value  $P_0$  to three values, 1, 5, and 15  
 421 MPa.  
 422

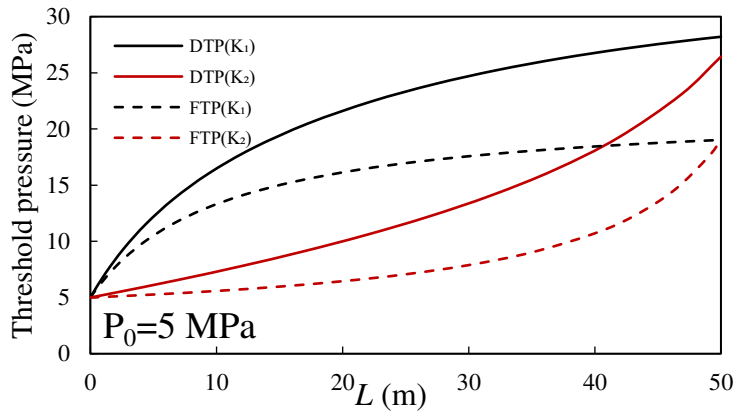


423  
 424  
 425 Figure 11. Schematic of method for calculating the threshold pressure distribution in one-dimensional  
 426 linear reservoir with permeability heterogeneity.  
 427

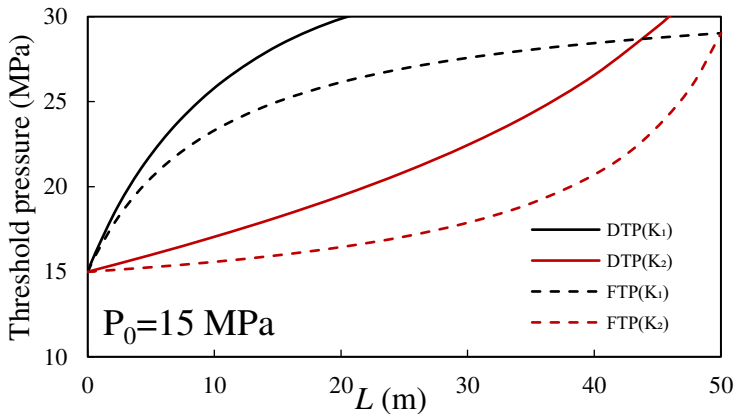
428 The calculated results of threshold pressure are compared with the results for a FTPG in Figure 12. The  
 429 effect of effective stress is not considered in the conventional TPG tests, the effective stress of the rock during  
 430 the tests is small. Consequently, the FTPG is taken as the value of  $DTPG_{min}(k)$  in Figure 4, and the FTPG is  
 431 only related to the permeability of rock <sup>[16,47]</sup>. The distribution of fixed threshold pressure (FTP) was  
 432 calculated based on  $DTPG_{min}(k)$ .  
 433



434



435



436

437

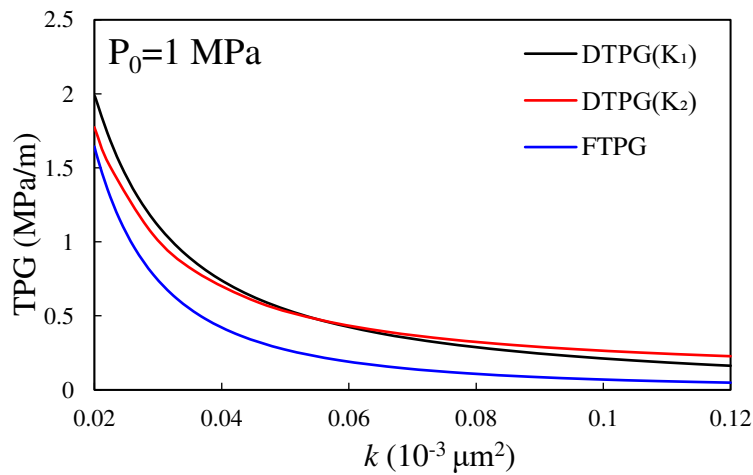
438 Figure 12. Threshold pressure distribution with length ( $L$ ) in heterogeneous reservoirs.  
 439 DTP is threshold pressure corresponding to the DTPG, FTP is the threshold pressure corresponding to the  
 440 FTPG.  $K_1$  represents a decreasing permeability along the flow direction,  $K_2$  represents an increasing  
 441 permeability along the flow direction. (The value of DTP+15MPa is over the overburden pressure 31MPa  
 442 when  $L > 20$  m for  $K_1$  and  $L > 46$  m for  $K_2$ , the 15 MPa curves of DTP are short.)  
 443

444 As shown in Figure 12, the FTP of the permeability distribution  $K_1$  increases rapidly with  $L$ , and then  
 445 increases slowly. The FTP of the permeability distribution  $K_2$  first increases slowly with  $L$ , and then increases  
 446 rapidly towards the production end. The shape of the FTP- $L$  curves is the same at different mean pore fluid

447 pressures. The total threshold pressure that needs to be overcome to start the flow of gas-water in the reservoir  
 448 is the same, which is 15 MPa ( $P_e - P_0$ ), regardless of the value of  $P_0$ . The shape of DTP- $L$  curve is similar to  
 449 that of the FTP- $L$  curve, while the values of DTP are larger than FTP.

450 Figure 13 shows the relationship between the DTPG and FTPG and the permeability at  $P_0=1$  MPa and  
 451 at  $P_{emin}$  for the permeability distributions  $K_1$  and  $K_2$ . The TPG values of rocks with the same permeability are  
 452 different for the two different permeability distributions,  $K_1$  and  $K_2$ . This is because the effective stress varies  
 453 according to location differently for the two permeability distributions, irrespective of the rock having the  
 454 same mean permeability. This results in the different values of  $P_{emin}$  in the reservoirs with different  
 455 heterogeneity.

456



457

458

459 Figure 13. Threshold pressure gradient (TPG) with rock permeability ( $k$ ) in the permeability distribution  
 460 mode  $K_1$  and  $K_2$  at  $P_0=1$  MPa and at  $P_{emin}$ .

461

462 In particular,  $P_{emin}$  of permeability distribution  $K_1$  is greater than that of permeability distribution  $K_2$   
 463 (Figure 12). The  $P_{emin}$  of  $K_1$  are 2.2 MPa larger than that of  $K_2$  at  $P_0=1$ , and 1.8 MPa at  $P_0=5$  MPa, respectively.

464 This is because the pore fluid pressure ( $P$ ) value is small at the production end, the corresponding  $P_{eff}$  value  
 465 is large, and the  $P_{eff}$  value is the largest at  $L=0$  m. Consequently, the rock DTPG sensitivity at the production  
 466 end is affected by a large stress. In the case of permeability distribution mode  $K_1$ , the DTPG values are large  
 467 and the DTPG stress sensitivity is strong at the production end due to the small rock permeability. In the case  
 468 of permeability distribution mode  $K_2$ , the rock permeability at the production end is large. The DTPG has a  
 469 relatively weak sensitivity to stress at the production end, these rocks have a relatively small DTPG values.

469

470 The overall result is that the total threshold pressure for 50 m reservoir of permeability distribution  $K_1$  is

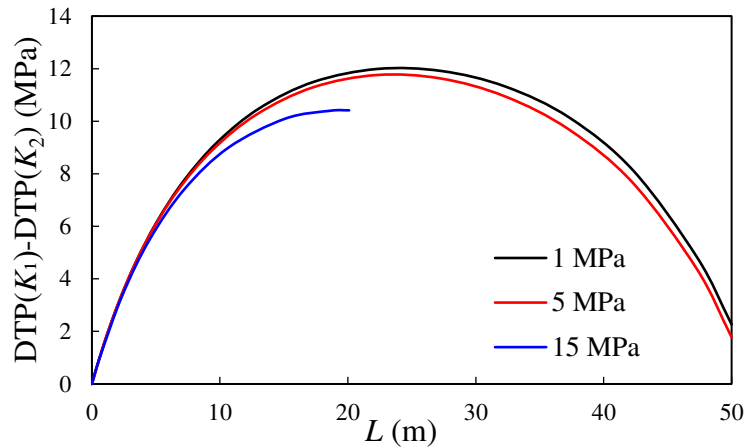
471 greater than that of  $K_2$ . Furthermore, this difference in threshold pressure between  $K_1$  and  $K_2$  is smaller at  
472 high reservoir pressures. This is due to the weak stress sensitivity of rock DTPG at high pore fluid pressures.

473 Consequently, the production well should be set at the position with high permeability. The gas flows  
474 from the position with low permeability to the position with high permeability, to reduce the overall threshold  
475 pressure. The differences in permeability distributions have less effect on the resulting total threshold  
476 pressure at higher pressures than that at lower pressures. However, when  $P_0$  is higher than a certain value  
477 (for example,  $P_0=15$  MPa), the total threshold pressure value in the  $K_1$  permeability distribution is larger than  
478 the maximum displacement differential pressure ( $P_e<31$  MPa) at a small  $L$  value. The gas in the reservoir at  
479  $L>20$  m cannot start to flow. In the case of  $K_2$  distribution mode, threshold pressure is smaller than maximum  
480 displacement differential pressure at  $L<46$  m. The gas production area is larger in reservoirs with  $K_2$ -type  
481 permeability distribution. More specific data of difference in threshold pressure between  $K_1$  and  $K_2$   
482 distributions ( $\Delta$ DTP- $L$  curve) is shown in Figure 14.

483 Interestingly, the inference made above that the production well should be set at the position with high  
484 permeability, is the same inference that has been arrived at using Advanced Fractal Reservoir Modelling  
485 (AFRM) of heterogeneous and anisotropic reservoirs [48-49]. In this research production optimization was  
486 tested for well placement randomly, and for all combinations of injection and production wells deliberately  
487 placed in fractally-distributed range of permeabilities from low to high permeability [50]. The results showed  
488 that best production occurred when both injection and production wells were deliberately placed in high  
489 permeability rocks [51].

490 The  $\Delta$ DTP- $L$  curve showed a trend of rapid increase at first and then a rapid decrease. The  $K_1$   
491 permeability distribution mode is unfavorable for gas flow, especially at a high  $P_0$  (for example,  $P_0=15$   
492 MPa). Because the value of total threshold pressure reaches the maximum differential pressure within a short  
493 distance from the production end. The gas cannot start to flow without additional fluid injection (such as  $\text{CO}_2$   
494 injection). On the other hand, a large  $P_0$  means a small value of the whole effective stress of the reservoir  
495 rock, and a small  $\Delta$ DTP value. Consequently, the selection of the production end  $P_0$  cannot be too large or  
496 too small, and there is a moderate value.

497



498

499

500 Figure 14. Difference in dynamic threshold pressure (DTP) distribution between  $K_1$  and  $K_2$  with length at  
 501 different values of  $P_0$ .

502

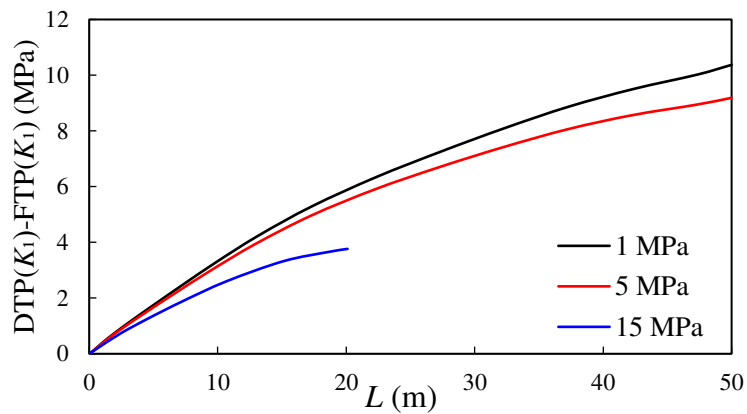
503 The difference between DTP and FTP in case of distribution  $K_1$  is shown in Figure 15. This difference

504 increases with  $L$ , and the difference becomes smaller at higher  $P_0$ . It shows that when the TPG is considered

505 to be a fixed value, a large well spacing results in a large prediction error of threshold pressure, and the error

506 is smaller at higher pressures.

507



508

509

510 Figure 15. Difference between dynamic threshold pressure (DTP) distribution and fixed threshold pressure  
 511 (FTP) distribution with length ( $L$ ) in  $K_1$  distribution at different values of  $P_0$ .

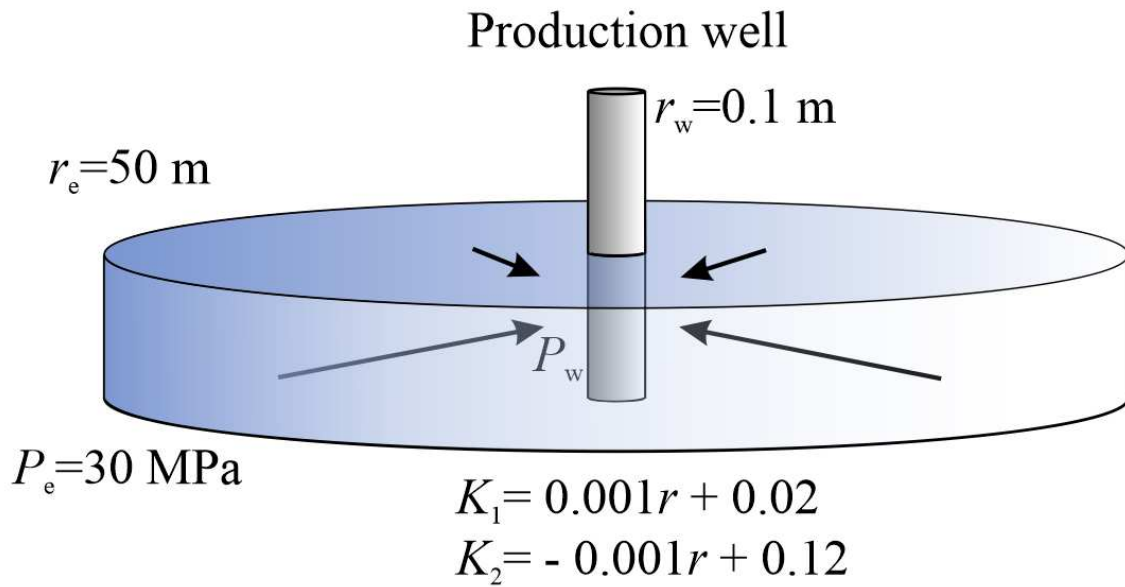
## 512 Gas production loss

513 The TPG needs to be overcome before production can start, and in a sense, it consumes a certain displacement

514 differential pressure, resulting in a part of gas production loss of the reservoir. As we have seen, there are

515 differences in the distribution of FTPG and DTPG in heterogeneous reservoirs. Traditionally, the prediction  
 516 of gas well production loss based on a FTPG value inevitably leads to deviations from expected production  
 517 values. The results exhibited previously in this paper indicate that the predicted value of the production loss  
 518 has conventionally been underestimated.

519 In order to explore the impact of DTPG and reservoir permeability heterogeneity on gas production  
 520 capacity loss in heterogeneous reservoirs, a cylindrical coordinate, horizontal and equal-thickness  
 521 heterogeneity model has been established. Once again, we have explored the results from two permeability  
 522 distributions,  $K_1$  and  $K_2$ . The production well is in the centre of the model, as shown in Figure 16.



523  
 524  
 525 Figure 16. Schematic diagram of a heterogeneous reservoir. The black arrows represent the flow direction,  
 526  $r_e$  is the radius of the model,  $P_e$  is the pressure at the edge of the reservoir,  $r_w$  is the radius of the gas  
 527 production well,  $P_w$  is the bottom hole flowing pressure,  $K_1$  represents a decreasing permeability  
 528 distribution towards the production well, and  $K_2$  represents an increasing permeability distribution towards  
 529 the production well.

530  
 531 The gas flow at radius  $r$  in the reservoir is [52],

532

$$q_0 = \frac{2\pi r h K_g}{\mu} \frac{dp}{dr} \quad (\text{Without TPG})$$

533

$$q_1 = \frac{2\pi r h K_g}{\mu} \left( \frac{dp}{dr} - \Delta P_{\text{thresh-F}} \right) \quad (\text{FTPG})$$

534

$$q_2 = \frac{2\pi r h K_g}{\mu} \left( \frac{dp}{dr} - \Delta P_{\text{thresh-K}_1}(P) \right) \quad (\text{DTPG-K}_1)$$

535

$$q_3 = \frac{2\pi r h K_g}{\mu} \left( \frac{dp}{dr} - \Delta P_{\text{thresh-K}_2}(P) \right) \quad (\text{DTPG-K}_2)$$

536 (6)

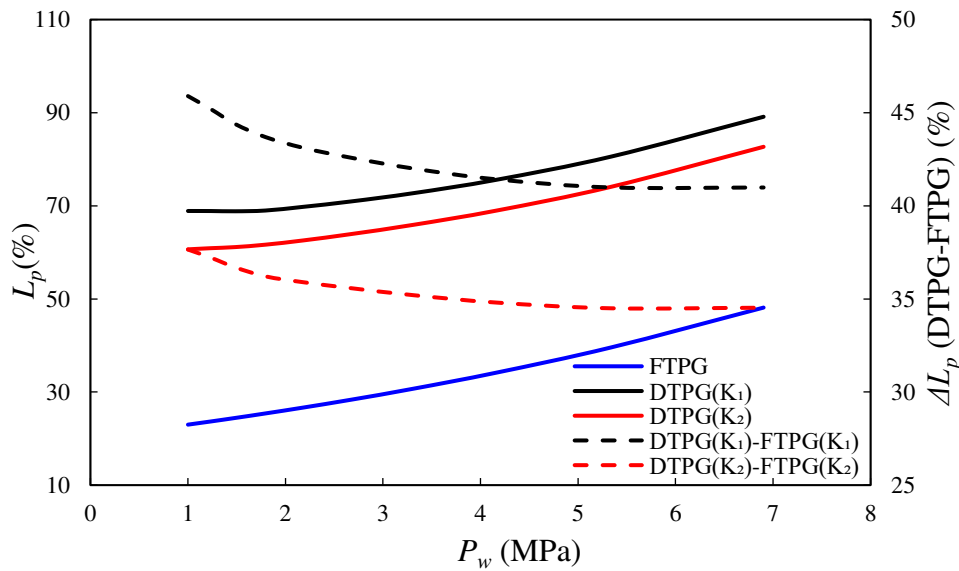
537 The gas well production  $Q_0$  without TPG is used as the benchmark, the gas well production loss caused  
 538 by TPG is,

$$539 L_p(\%) = (100 - \frac{Q}{Q_0} \times 100) \quad (7)$$

540 where  $q_0, q_1, q_2, q_3$  are the gas flows for each scenario ( $m^3/s$ ),  $h$  is the reservoir thickness (m),  $L_p$  is the gas  
 541 well production loss ratio (%), and  $Q$  is the gas well production ( $m^3/d$ ).

542 We combine Eqs. (6) and (7) to calculate  $L_p$  of gas well at different  $P_w$  using MATLAB tool integration,  
 543 the result is shown in Figure 17.

544



545

546

547 Figure 16. The gas production loss ( $L_p$ ) due to DTPG and FTPG at different  $P_w$  in a heterogeneous  
 548 reservoir. DTPG is dynamic threshold pressure gradient, FTPG is fixed threshold pressure gradient, and  
 549  $\Delta L_p = L_p$  of DTPG  $- L_p$  of FTPG.)

550

551 As expected, as shown in Figure 17, the  $L_p$  of DTPG is much higher than that of FTPG, because the  
 552 value of DTPG is higher than that of FTPG. The difference in  $L_p$  ( $\Delta L_p$ ) between DTPG and FTPG is 40-45%  
 553 at  $P_w$  of 1 to 7 MPa in the permeability distribution  $K_1$ , and  $\Delta L_p$  is 34-37% in permeability distribution  $K_2$ .  
 554 The value of  $\Delta L_p$  gradually decreases as  $P_w$  increases, but tends to a constant value at high values of  $P_w$ . If  
 555 the TPG is considered to be fixed, large prediction errors of gas well production results, especially at lower  
 556  $P_w$ . Moreover,  $L_p$  increases with  $P_w$ , this is due to the fact that a large  $P_w$  means a small displacement  
 557 differential pressure ( $P_e - P_w$ ). The threshold pressure as the loss of displacement differential pressure accounts

558 for a large proportion of the total displacement differential pressure [22]. The  $L_p$  of FTPG is 23-48%, that is,  
559 over 20% even at the minimum  $P_w$ . The threshold pressure has a greater impact on gas well production in  
560 tight gas reservoirs. When the production differential pressure is small, the threshold pressure makes more  
561 gas reserves unproducibile from the reservoir. The effective development of gas cannot be maintained only  
562 by relying on the initial pressure of the reservoir.

563 Furthermore, the increase trend of  $L_p$ - $P_w$  is slow first and then fast in Figure 16. On the one hand, a high  
564  $P_w$  results in a small DTPG. On the other hand, a high  $P_w$  results in a large  $L_p$ . This  $L_p$ - $P_w$  behavior is  
565 controlled by two opposing factors. It is worth noting that, the value of  $L_p$  in the permeability distribution  
566  $K_1$  is higher than that in the permeability distribution  $K_2$ . It demonstrates that the permeability distribution  
567 mode  $K_1$  is unfavorable for the development of tight gas reservoir, which causes the gas in a wider range of  
568 reservoirs to be unable to flow.

## 569 Conclusions

570 In this paper, we tested the DTPG values on cores with different permeability at different stresses and  
571 saturations of mobile water. The quantitative relationship between permeability and the DTPG sensitivity  
572 coefficients was studied. The threshold pressure distributions of different permeability distribution modes of  
573 tight gas reservoirs were calculated based on our experimental data, and the gas production loss of DTPG  
574 and FTPG were compared. We obtained the following conclusions based on our experiments:

- 575 (1) The DTPG of tight gas reservoir rocks increases logarithmically by 0.5-3.9 times in the effective stress  
576 range of 0.6-30.5 MPa, such that rocks with smaller permeability exhibit a stronger stress sensitivity of DTPG.
- 577 (2) The DTPG of tight gas reservoir rocks increases exponentially by 2.7-6.5 times from irreducible water  
578 saturation to a mobile water saturation of 25%. Once again, rocks with smaller permeability exhibited a  
579 stronger mobile water saturation sensitivity of DTPG.
- 580 (3) The distribution of increasing permeability in the displacement direction is beneficial to the reduction of  
581 the threshold pressure. The influence of the reservoir permeability heterogeneity on the DTPG is smaller at  
582 higher pressure.
- 583 (4) DTPG causes a 34-45% higher gas production loss in tight reservoirs than FTPG. The distribution of  
584 decreasing permeability in the displacement direction makes a 6-8% larger gas production loss than that of  
585 an opposite permeability distribution.

586 Overall, the sensitivity of DTPG to stress and mobile water shows decreasing trends with rock  
587 permeability. The threshold pressure is small when the direction of gas flow is consistent with the direction  
588 of increasing permeability in heterogeneous reservoirs. Production wells should be located in high  
589 permeability sections of heterogeneous reservoirs to reduce the threshold pressure.

## 590 List of main abbreviations

591	TPG	Threshold pressure gradient
592	DTPG	Dynamic threshold pressure gradient
593	DTPG	Fixed threshold pressure gradient
594	DTP	Dynamic threshold pressure
595	FTP	Fixed threshold pressure
596	$DTPG_{\min}$	DTPG value at minimum effective stress of rock
597	$DTPG_{\max}$	DTPG value at maximum effective stress of rock
598	$P_{eff}$	Rock effective stresses
599	$\lambda$	Stress sensitivity coefficient of threshold pressure gradient
600	$\eta$	Mobile water sensitivity coefficient of threshold pressure gradient
601	$S_{wi}$	Irreducible water saturation
602	$k$	Core permeability
603	$S_m$	Mobile water saturation
604	$P_o$	Overburden pressure
605	$P_0$	Pressure at production end
606	$P_e$	Pressure at reservoir edge
607	$K_1$	A decreasing permeability distribution mode along the flow direction
608	$K_2$	An increasing permeability distribution mode along the flow direction
609	$L$	Distance from the production well
610	$P_{emin}$	A minimum $P_e$ value, which is just large enough for the gas to start flowing
611	$P_w$	Bottom hole flowing pressure
612	$L_p$	Gas production loss
613	$\Delta L_p$	Difference in production loss between dynamic and fixed threshold pressure gradient

## 614 Acknowledgments

615 This research is supported by National Natural Science Foundation of China, “The formation mechanism of  
616 residual gas and liquid in coal seam and the geological constraints for effective production” (41872171), and  
617 “Cross-scale precipitation mode of asphaltene in ultra-deep sandstone reservoir during CO<sub>2</sub> flooding”  
618 (52104048).

## References

- 620 [1] Wei, J and Wang, K., 2018. A preliminary study of the present-day in-situ stress state in the Ahe tight gas  
621 reservoir, Dibeig Gasfield, Kuqa Depression. *Marine and Petroleum Geology* 96: 154-165.
- 622 [2] Oluwadabi, A. G., Taylor, K.G and Ma, L., 2019. A case study on 3D characterisation of pore structure in  
623 a tight sandstone gas reservoir: the Collyhurst Sandstone, East Irish Sea Basin, northern England. *Journal of*  
624 *Natural Gas Science and Engineering* 68: 102917.
- 625 [3] Huang, H., Babadagli, T., Chen, X., Li, H., & Zhang, Y., 2020. Performance comparison of novel chemical  
626 agents for mitigating water-blocking problem in tight gas sandstones. *SPE Reservoir Evaluation &*  
627 *Engineering* 23.04: 1150-1158.
- 628 [4] Nazari, M. H., Tavakoli, V., Rahimpour-Bonab, H., & Sharifi-Yazdi, M., 2019. Investigation of factors  
629 influencing geological heterogeneity in tight gas carbonates, Permian reservoir of the Persian Gulf. *Journal*  
630 *of Petroleum Science and Engineering*, 183, 106341.
- 631 [5] Nelson, P. H., 2009. Pore-throat sizes in sandstones, tight sandstones, and shales. *AAPG bulletin*, 93(3),  
632 329-340.
- 633 [6] Hu, H., Zeng, Z., & Liu, J., 2015. Key elements controlling oil accumulation within the tight  
634 sandstones. *Journal of Earth Science*, 26(3), 328-342.
- 635 [7] Wang, J., Wu, S., Li, Q., Zhang, J., & Guo, Q., 2020. Characterization of the pore-throat size of tight oil  
636 reservoirs and its control on reservoir physical properties: A case study of the Triassic tight sandstone of the  
637 sediment gravity flow in the Ordos Basin, China. *Journal of Petroleum Science and Engineering*, 186,  
638 106701.
- 639 [8] Zafar, A., Su, Y. L., Li, L., Fu, J. G., Mehmood, A., Ouyang, W. P., & Zhang, M., 2020. Tight gas  
640 production model considering TPG as a function of pore pressure, permeability and water saturation.  
641 *Petroleum Science*, 17(5), 1356-1369.
- 642 [9] Zhao, F., Liu, P., Hao, S., Qiu, X., Shan, C., & Zhou, Y., 2021. A new dynamic capillary-number-recovery  
643 evaluation method for tight gas reservoirs. *Journal of Petroleum Science and Engineering*, 204, 108730.
- 644 [10] Zeng, J., Wang, X., Guo, J., Zeng, F., & Zhang, Q., 2018. Composite linear flow model for multi-  
645 fractured horizontal wells in tight sand reservoirs with the threshold pressure gradient. *Journal of Petroleum*  
646 *Science and Engineering*, 165, 890-912.
- 647 [11] Tian, W., Li, A., Ren, X., & Josephine, Y., 2018. The threshold pressure gradient effect in the tight  
648 sandstone gas reservoirs with high water saturation. *Fuel*, 226, 221-229.
- 649 [12] Song, H., Cao, Y., Yu, M., Wang, Y., Killough, J. E., & Leung, J., 2015. Impact of permeability  
650 heterogeneity on production characteristics in water-bearing tight gas reservoirs with threshold pressure  
651 gradient. *Journal of Natural Gas Science and Engineering*, 22, 172-181.
- 652 [13] Wang, Q., Yang, S., Glover, P. W., Lorinczi, P., Qian, K., & Wang, L., 2020. Effect of pore-throat  
653 microstructures on formation damage during miscible CO<sub>2</sub> flooding of tight sandstone reservoirs. *Energy &*  
654 *Fuels*, 34(4), 4338-4352.
- 655 [14] Wang, Q., Wang, L., Glover, P. W., & Lorinczi, P., 2020. Effect of a Pore Throat Microstructure on  
656 Miscible CO<sub>2</sub> Soaking Alternating Gas Flooding of Tight Sandstone Reservoirs. *Energy & Fuels*, 34(8),  
657 9450-9462.
- 658 [15] Zafar, A., Su, Y. L., Li, L., Fu, J. G., Mehmood, A., Ouyang, W. P., & Zhang, M., 2020. Tight gas  
659 production model considering TPG as a function of pore fluid pressure, permeability and water  
660 saturation. *Petroleum Science*, 17(5), 1356-1369.

- 661 [16] Warpinski, N. R., & Teufel, L. W., 1992. Determination of the effective-stress law for permeability and  
662 deformation in low-permeability rocks. *SPE Formation Evaluation*, 7(02), 123-131.
- 663 [17] Zhu, W., Song, H., Huang, X., Liu, X., He, D., & Ran, Q., 2011. Pressure characteristics and effective  
664 deployment in a water-bearing tight gas reservoir with low-velocity non-Darcy flow. *Energy & Fuels*, 25(3),  
665 1111-1117.
- 666 [18] Ding, J., Yang, S., Nie, X., & Wang, Z., 2014. Dynamic threshold pressure gradient in tight gas  
667 reservoir. *Journal of Natural Gas Science and Engineering*, 20, 155-160.
- 668 [19] Liu, K., Yin, D. and Su, H., 2020. Transient transfer shape factor for fractured tight reservoirs: Effect of  
669 the dynamic threshold pressure gradient in unsteady flow. *Energy Science & Engineering*, 8(7), pp. 2566-  
670 2586.
- 671 [20] Liu, K., Yin, D., Sun, Y. and Xia, L., 2020. Analytical and experimental study of stress sensitivity effect  
672 on matrix/fracture transfer in fractured tight reservoir. *Journal of Petroleum Science and Engineering*, 195,  
673 p. 107958.
- 674 [21] Wang, X. and Sheng, J.J., 2017. Discussion of liquid threshold pressure gradient. *Petroleum*, 3(2), pp.  
675 232-236.
- 676 [22] Wang, Q., Zhu, B., Shen, J., Glover, P. W., Lorinczi, P., & Han, H., 2022. Quantifying Controls on  
677 Threshold Pressure during CO<sub>2</sub> Injection in Tight Gas Reservoir Rocks. *Energy & Fuels*.
- 678 [23] Cao, L. N., Li, X. P., Luo, C., Yuan, L., Zhang, J. Q., & Tan, X. H., 2016. Horizontal well transient rate  
679 decline analysis in low permeability gas reservoirs employing an orthogonal transformation method. *Journal*  
680 *of Natural Gas Science and Engineering*, 33, 703-716.
- 681 [24] Bo, N., Zuping, X., Xianshan, L., Zhijun, L., Zhonghua, C., Bocai, J., & Xiaolong, C., 2020. Production  
682 prediction method of horizontal wells in tight gas reservoirs considering threshold pressure gradient and  
683 stress sensitivity. *Journal of Petroleum Science and Engineering*, 187, 106750.
- 684 [25] Song, H., Liu, Q., Yang, D., Yu, M., Lou, Y., & Zhu, W., 2014. Production equation of fractured horizontal  
685 well in a water-bearing tight gas reservoir with low-velocity non-Darcy flow. *Journal of Natural Gas Science*  
686 *and Engineering*, 18, 467-473.
- 687 [26] Glover, P.W.J. and Luo, M., 2020. The Porosity and Permeability of Binary Grain Mixtures. *Transport*  
688 *in Porous Media*, 132(1), pp. 1-37.
- 689 [27] Walker, E. and Glover, P.W.J., 2010. Permeability models of porous media: Characteristic length scales,  
690 scaling constants and time-dependent electrokinetic coupling. *Geophysics*, 75(6), pp. E235-E246.
- 691 [28] Glover, P.W.J. and Walker, E., 2009. Grain-size to effective pore-size transformation derived from  
692 electrokinetic theory. *Geophysics*, 74(1), pp. E17-E29.
- 693 [29] Garum, M., Glover, P.W.J., Lorinczi, P., Scott, G. and Hassanpour, A., 2021. Ultrahigh-Resolution 3D  
694 Imaging for Quantifying the Pore Nanostructure of Shale and Predicting Gas Transport. *Energy and Fuels*,  
695 35(1), pp. 702-717.
- 696 [30] Garum, M., Glover, P.W.J., Lorinczi, P., Micklethwaite, S. and Hassanpour, A., 2021. Integration of  
697 Multiscale Imaging of Nanoscale Pore Microstructures in Gas Shales. *Energy and Fuels*, 35(13), pp. 10721-  
698 10732.
- 699 [31] Ding, J., Yang, S., Cao, T., & Wu, J., 2018. Dynamic threshold pressure gradient in tight gas reservoir  
700 and its influence on well production. *Arabian Journal of Geosciences*, 11(24), 1-6.
- 701 [32] Fu, J., Su, Y., Li, L., Wang, W., Wang, C., & Li, D., 2022. Production model with mechanisms of multiple  
702 seepage in tight gas reservoir. *Journal of Petroleum Science and Engineering*, 209, 109825.
- 703 [33] Wu, Z., Cui, C., Lv, G., Bing, S., & Cao, G., 2019. A multi-linear transient pressure model for multistage  
704 fractured horizontal well in tight oil reservoirs with considering threshold pressure gradient and stress

705 sensitivity. *Journal of Petroleum Science and Engineering*, 172, 839-854.

706 [34] Lu, C., Qin, X., Ma, C., Yu, L., Geng, L., Bian, H., & Zhou, Y., 2022. Investigation of the impact of  
707 threshold pressure gradient on gas production from hydrate deposits. *Fuel*, 319, 123569.

708 [35] Liu, G., Xie, S., Tian, W., Wang, J., Li, S., Wang, Y., & Yang, D., 2022. Effect of pore-throat structure  
709 on gas-water seepage behaviour in a tight sandstone gas reservoir. *Fuel*, 310, 121901.

710 [36] Wang, C., Cheng, Y., Yi, M., Jiang, J., & Wang, D., 2021. Threshold pressure gradient for helium seepage  
711 in coal and its application to equivalent seepage channel characterization. *Journal of Natural Gas Science  
712 and Engineering*, 96, 104231.

713 [37] Liu, B., Yang, Y., Li, J., Chi, Y., Li, J., & Fu, X., 2020. Stress sensitivity of tight reservoirs and its effect  
714 on oil saturation: A case study of Lower Cretaceous tight clastic reservoirs in the Hailar Basin, Northeast  
715 China. *Journal of Petroleum Science and Engineering*, 184, 106484.

716 [38] Zeng, J., Wang, X., Guo, J., & Zeng, F., 2016, August. Analytical model for multi-fractured horizontal  
717 wells in tight sand reservoir with threshold pressure gradient. In *SPE Asia Pacific Hydraulic Fracturing  
718 Conference*. OnePetro.

719 [39] Dou, X., Liao, X., Zhao, X., Wang, H., & Lv, S., 2015. Quantification of permeability stress-sensitivity  
720 in tight gas reservoir based on straight-line analysis. *Journal of Natural Gas Science and Engineering*, 22,  
721 598-608.

722 [40] Liu, G., Yin, H., Lan, Y., Fei, S., & Yang, D., 2020. Experimental determination of dynamic pore-throat  
723 structure characteristics in a tight gas sandstone formation with consideration of effective stress. *Marine and  
724 Petroleum Geology*, 113, 104170.

725 [41] Liu, G., Wang, Y., Yin, H., Ding, Y., Lan, Y., & Yang, D., 2022. Determination of gas-water seepage  
726 characteristics with consideration of dynamic pore-throat structure in a tight sandstone gas formation. *Marine  
727 and Petroleum Geology*, 136, 105440.

728 [42] Shi, H., Lai, F., Shi, G., Liang, Y., & Dai, Y., 2021. Dynamic prediction and influencing factors analysis  
729 of gas and water co-production stage in tight sandstone reservoir. *Journal of Natural Gas Science and  
730 Engineering*, 96, 104327.

731 [43] Zeng, J., Zhang, Y., Zhang, S., Qiao, J., Feng, X., & Feng, S., 2016. Experimental and theoretical  
732 characterization of the natural gas migration and accumulation mechanism in low-permeability (tight)  
733 sandstone cores. *Journal of Natural Gas Science and Engineering*, 33, 1308-1315.

734 [44] Yang, X., Meng, Y., Shi, X., & Li, G., 2017. Influence of porosity and permeability heterogeneity on  
735 liquid invasion in tight gas reservoirs. *Journal of Natural Gas Science and Engineering*, 37, 169-177.

736 [45] Qu, Y., Sun, W., Tao, R., Luo, B., Chen, L., & Ren, D., 2020. Pore-throat structure and fractal  
737 characteristics of tight sandstones in Yanchang Formation, Ordos Basin. *Marine and Petroleum Geology*, 120,  
738 104573.

739 [46] Cheng, Y., Zhang, C., & Zhu, L. Q., 2017. A fractal irreducible water saturation model for capillary tubes  
740 and its application in tight gas reservoir. *Journal of Petroleum Science and Engineering*, 159, 731-739.

741 [47] Dong, M., Shi, X., Ling, S., Zhang, B., & Li, X., 2019. Effect of dynamic pseudo threshold pressure  
742 gradient on well production performance in low-permeability and tight oil reservoirs. *Journal of Petroleum  
743 Science and Engineering*, 173, 69-76.

744 [48] Al-Zainaldin, S., Glover, P.W.J. and Lorinczi, P., 2017. Synthetic Fractal Modelling of Heterogeneous  
745 and Anisotropic Reservoirs for Use in Simulation Studies: Implications on Their Hydrocarbon Recovery  
746 Prediction. *Transport in Porous Media*, 116(1), pp. 181-212.

- 747 [49] Glover, P.W.J., Lorinczi, P., Al-Zainaldin, S., Al-Ramadhan, H., Sinan, S. and Daniel, G., 2019. A  
748 fractal approach to the modelling and simulation of heterogeneous and anisotropic reservoirs, *Society of*  
749 *Petroleum Engineers - SPE Offshore Europe Conference and Exhibition 2019*, OE 2019.
- 750 [50] Glover, P.W.J., Lorinczi, P., Al-Zainaldin, S., Al-Ramadan, H., Daniel, G. and SINAN, S., 2018.  
751 Advanced fractal modelling of heterogeneous and anisotropic reservoirs, *SPWLA 59th Annual Logging*  
752 *Symposium* 2018.
- 753 [51] Sinan, S., Glover, P.W.J. and Lorinczi, P., 2020. Modelling the Impact of Anisotropy on Hydrocarbon  
754 Production in Heterogeneous Reservoirs. *Transport in Porous Media*, 133(3), pp. 413-436.
- 755 [52] Diwu, P., Liu, T., You, Z., Jiang, B., & Zhou, J., 2018. Effect of low velocity non-Darcy flow on pressure  
756 response in shale and tight oil reservoirs. *Fuel*, 216, 398-406.
- 757